

Ozone oxidation of 4H-SiC and flat-band voltage stability of SiC MOS capacitors

Zhi-Peng Yin(尹志鹏), Sheng-Sheng Wei(尉升升), Jiao Bai(白娇), Wei-Wei Xie(谢威威), Zhao-Hui Liu(刘兆慧), Fu-Wen Qin(秦福文), and De-Jun Wang(王德君)

Citation: Chin. Phys. B, 2022, 31 (**11**): 117302. DOI: 10.1088/1674-1056/ac7ccf

What follows is a list of articles you may be interested in

Dependence of short channel length on negative/positive bias temperature instability (NBTI/PBTI) for 3D FinFET devices

Ren-Ren Xu(徐忍忍), Qing-Zhu Zhang(张青竹), Long-Da Zhou(周龙达), Hong Yang(杨红), Tian-Yang Gai(盖天洋), Hua-Xiang Yin(殷华湘), and Wen-Wu Wang(王文武)

Chin. Phys. B, 2022, 31 (**1**): 017301. DOI: 10.1088/1674-1056/ac1410

Influence of ultra-thin TiN thickness (1.4 nm and 2.4 nm) on positive bias temperature instability (PBTI) of high-*k*/metal gate nMOSFETs with gate-last process

Qi Lu-Wei (祁路伟), Yang Hong (杨红), Ren Shang-Qing (任尚清), Xu Ye-Feng (徐烨峰), Luo Wei-Chun (罗维春), Xu Hao (徐昊), Wang Yan-Rong (王艳蓉), Tang Bo (唐波), Wang Wen-Wu (王文武), Yan Jiang (闫江), Zhu Hui-Long (朱慧珑), Zhao Chao (赵超), Chen Da-Peng (陈大鹏), Ye Tian-Chun (叶甜春)

Chin. Phys. B, 2015, 24 (**12**): 127305. DOI: 10.1088/1674-1056/24/12/127305

Recovery of PMOSFET NBTI under different conditions

Cao Yan-Rong (曹艳荣), Yang Yi (杨毅), Cao Cheng (曹成), He Wen-Long (何文龙), Zheng Xue-Feng (郑雪峰), Ma Xiao-Hua (马晓华), Hao Yue (郝跃)

Chin. Phys. B, 2015, 24 (**9**): 097304. DOI: 10.1088/1674-1056/24/9/097304

Energy distribution extraction of negative charges responsible for positive bias temperature instability

Ren Shang-Qing (任尚清), Yang Hong (杨红), Wang Wen-Wu (王文武), Tang Bo (唐波), Tang Zhao-Yun (唐兆云), Wang Xiao-Lei (王晓磊), Xu Hao (徐昊), Luo Wei-Chun (罗维春), Zhao Chao (赵超), Yan Jiang (闫江), Chen Da-Peng (陈大鹏), Ye Tian-Chun (叶甜春)

Chin. Phys. B, 2015, 24 (**7**): 077304. DOI: 10.1088/1674-1056/24/7/077304

Flat-roof phenomenon of dynamic equilibrium phase in the negative bias temperature instability effect on a power MOSFET

Zhang Yue (张月), Zhuo Qing-Qing (卓青青), Liu Hong-Xia (刘红侠), Ma Xiao-Hua (马晓华), Hao Yue (郝跃)

Chin. Phys. B, 2014, 23 (**5**): 057304. DOI: 10.1088/1674-1056/23/5/057304

Ozone oxidation of 4H-SiC and flat-band voltage stability of SiC MOS capacitors

Zhi-Peng Yin(尹志鹏)[1], Sheng-Sheng Wei(尉升升)[1], Jiao Bai(白娇)[1], Wei-Wei Xie(谢威威)[1], Zhao-Hui Liu(刘兆慧)[1], Fu-Wen Qin(秦福文)[2], and De-Jun Wang(王德君)[1,†]

[1] *Key Laboratory of Intelligent Control and Optimization for Industrial Equipment, Ministry of Education; School of Control Science and Engineering, Faculty of Electronic Information and Electrical Engineering, Dalian University of Technology, Dalian* 116024, *China*

[2] *State Key Laboratory of Materials Modification by Laser, Ion, and Electron Beams (Ministry of Education), Dalian University of Technology, Dalian* 116024, *China*

(Received 19 May 2022; revised manuscript received 28 June 2022; accepted manuscript online 29 June 2022)

We investigate the effect of ozone (O_3) oxidation of silicon carbide (SiC) on the flat-band voltage (V_{fb}) stability of SiC metal–oxide–semiconductor (MOS) capacitors. The SiC MOS capacitors are produced by O_3 oxidation, and their V_{fb} stability under frequency variation, temperature variation, and bias temperature stress are evaluated. Secondary ion mass spectroscopy (SIMS), atomic force microscopy (AFM), and x-ray photoelectron spectroscopy (XPS) indicate that O_3 oxidation can adjust the element distribution near SiC/SiO_2 interface, improve SiC/SiO_2 interface morphology, and inhibit the formation of near-interface defects, respectively. In addition, we elaborate the underlying mechanism through which O_3 oxidation improves the V_{fb} stability of SiC MOS capacitors by using the measurement results and O_3 oxidation kinetics.

Keywords: SiC MOS capacitors, ozone oxidation, bias temperature instability, Deal–Grove model

PACS: 73.61.Ey, 73.40.Qv, 81.65.Mq, 85.30.De **DOI:** 10.1088/1674-1056/ac7ccf

1. Introduction

Silicon carbide (SiC) and gallium nitride (GaN) materials are the third-generation semiconductors. However, unlike the application of GaN device in high frequency field,[1–4] SiC power device is more favored in the field of high temperature and high voltage due to its wide bandgap, high breakdown field strength, high thermal conductivity, and high compatibility with the Si process.[1,2] However, the low channel mobility and threshold voltage (V_{th}) instability of SiC metal–oxide–semiconductor field-effect-transistor (MOSFET) device seriously limit its development.[3,4] After decades of research, although the channel mobility of SiC MOSFET device has been improved to an acceptable level via the nitric oxide (NO) post-oxidation annealing (POA) process,[5,6] the V_{th} instability of SiC MOS capacitor is still a serious problem to be solved.[7] The V_{th}/flat-band voltage (V_{fb}) instability is mainly due to the interface trap and near interface oxide trap (NIOT) formed near the interface during traditional dry oxidation.[8–10]

These defects can be eliminated by POA and improved oxidation processes;[5,11–13] the latter can suppress the generation of these defects fundamentally by increasing the oxidant concentration near the SiC/silicon dioxide (SiO_2) interface.[14–16] Improved oxidation processes include wet oxidation,[17] NO oxidation,[6] plasma oxidation,[18,19] and ozone (O_3) oxidation.[20] Although these methods can reduce the interface trap density (D_{it}) of SiC MOS devices to some extent, wet oxygen, NO, and plasma oxidation may lead to V_{th}/V_{fb} instability,[21,22] the introduction of fast traps,[23] and sample damage due to highly energetic particle bombardment,[24] respectively. By contrast, O_3 oxidation can inhibit the generation of interface defects without the introduction of foreign elements.[25] It has a low manufacturing cost for SiC MOS devices because of its high compatibility with Si oxidation, and is more environment friendly than NO.[26] In 2003, Kosugi *et al.* reported that O_3 oxidation of SiC can reduce the D_{it} of SiC MOS capacitors.[20] However, no further reports have been provided.

In this work, we investigate the V_{fb} stability of SiC MOS capacitor produced by O_3 oxidation. The V_{fb} stability of SiC MOS capacitor via current–voltage (I–V) measurement at room temperature and capacitance–voltage (C–V) measurements at different test temperatures, test frequencies, and bias temperature stresses are evaluated. Subsequently, secondary ion mass spectrometry (SIMS), atomic force microscopy (AFM), and x-ray photoelectron spectroscopy (XPS) are used to test the element distribution, interface morphology, and interface element bonding near the SiC/SiO_2 interface, respectively. The underlying mechanism through which O_3 oxidation affects the V_{fb} stability of SiC MOS capacitors is analyzed based on the measurement results and oxidation kinetics.

2. Experiment

The 4° off-axis n-type 4H-SiC substrates with 5-μm-thick epitaxial layers produced by Cree Inc., were used in this experiment. The epitaxial layers were doped with N concentration of 1×10^{16} cm^{-3}. The substrates were cleaned successively in

†Corresponding author. E-mail: dwang121@dlut.edu.cn

© 2022 Chinese Physical Society and IOP Publishing Ltd

acetone, ethanol, and deionized water via ultrasonic cleaning and immersed in 15% hydrofluoric acid (HF) buffer solution for 10 min to remove the natural oxide layer. Subsequently, the substrates were subjected to Radio Corporation of America standard cleaning and dried under the protection of N_2. The O_3 oxidation of SiC was carried out separately at oxidation temperatures of 1100 °C, 1150 °C, and 1200 °C to obtain 35-nm SiO_2 films.

The oxidant was O_3/O_2 mixed atmosphere with an O_3 concentration of 150 mg/L; it was produced via dielectric barrier discharge in high-purity O_2. Meanwhile, control samples were oxidized in high-purity O_2 atmosphere at 1200 °C to obtain 30-nm-thick SiO_2 films. All samples were annealed *in situ* in N_2 for 30 min. After removing the oxide film on the back of the samples, we evaporated aluminium (Al) on the front and back of each sample to create a gate electrode and back electrode, each with a diameter of 200 μm, respectively. The SiC MOS capacitors were prepared after electrodes have been metallized in N_2 atmosphere.

The Keithley 4200 semiconductor characterization system was used to evaluate the electrical characteristics of the various SiC MOS capacitors. The *I*–*V* measurement was performed to test the insulation characteristics of SiO_2 films on SiC. The *C*–*V* curves were extracted with different frequencies in a range from 10 kHz to 5 MHz at room temperature to study the frequency dispersion of the various SiC MOS capacitors. Subsequently, the temperature dependence of the V_{fb} of the SiC MOS capacitors was analyzed by using the *C*–*V* curves tested under different temperatures (from 80 K to 300 K). After exerting the positive and negative bias temperature stress (PBTS and NBTS), the *C*–*V* curves were measured at 100, 150, 200, and 300 K, and the stress value and stress time were ±2.5 MV/cm and 600 s, respectively. The bias temperature instability (BTI) of the various SiC MOS capacitors was evaluated by using the difference (ΔV_{fb}) between the V_{fb} values of the *C*–*V* curves after having exerted positive stress and negative stress. In addition, D_{it} and N_{ot} were extracted to study the mechanism through which O_3 oxidation affects the V_{fb} stability of SiC MOS capacitors.

The element distribution near the SiC/SiO_2 interface can considerably affect the type of defect near the SiC/SiO_2 interface. To understand the influence of O_3 oxidation on the element distribution near the SiC/SiO_2 interface, we performed the SIMS measurement of the SiC/SiO_2 structures to obtain the depth profile of Si, carbon (C), and O elements. The SiC/SiO_2 interface morphology and the chemical bonding state of interfacial Si and C were extracted through AFM and XPS, respectively. XPS Si 2p and C 1s spectra were obtained by using the PHI Quantera II system with a monochromatic Al Kα source ($h\nu = 1486.6$ eV). The results were utilized to evaluate the interface quality of different samples. In addition, the kinetics of O_3 oxidation was analyzed based on the modified Deal–Grove model presented by Yoshioka *et al.*[27] The model was combined with the measurement results to elucidate the underlying mechanism of the effect of O_3 oxidation on the V_{fb} stability of SiC MOS capacitors.

3. Results and discussion

3.1. Breakdown characteristics of SiO_2 films

Figure 1 shows the *J*–*E* curves of the SiC MOS capacitors and the breakdown field strength (E_{ox}) of the SiO_2 films. The *J*–*E* curves present the typical Fowler–Nordheim (FN) characteristics.[28] Although the leakage currents in the SiO_2 films of the various samples are similar in the soft breakdown region, obvious differences exist in the E_{ox} of the various samples. We extract the E_{ox} values of different samples as shown in Fig. 1(b). The E_{ox} increases with the rise of O_3 oxidation temperature, indicating that O_3 oxidation at high O_3 oxidation temperatures in a range of 1100 °C–1200 °C can produce SiO_2 films with good insulation characteristics. Compared with the SiO_2 films prepared via dry oxidation at the same oxidation temperature (1200 °C), the samples prepared by O_3 oxidation has a larger E_{ox}. This result indicates that the O_3 oxidation can produce SiO_2 films with good insulation characteristics, which is the precondition to achieve good V_{fb} stability in SiC MOS devices.[29]

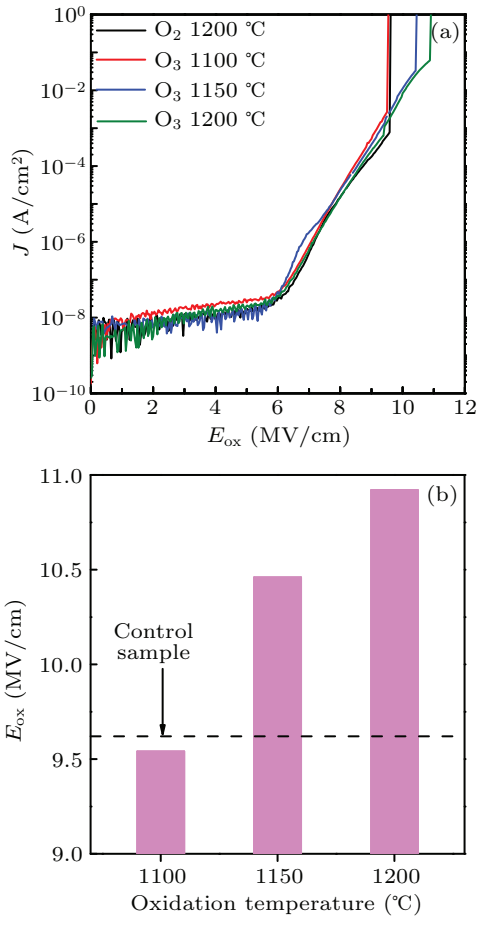


Fig. 1. (a) The *J*–*E* curves and (b) E_{ox} *versus* oxidation temperature of various SiC MOS capacitors, with dotted lines representing E_{ox} of SiO_2 film of the control sample.

3.2. Frequency dispersion

As shown in Fig. 2, we extract the *C*–*V* curves of the SiC MOS capacitors at different frequencies ranging from 10 kHz to 1 MHz. The *C*–*V* curves of all the samples gradually shift toward the accumulation region with the increase in test frequency; this phenomenon is called frequency dispersion.[30,31] We observed that large frequency dispersion leads to an obvious V_{fb} shift, that is, V_{fb} instability of the SiC MOS capacitors is induced by test frequency variation. As shown in Fig. 2, the frequency dispersions of the various SiC MOS capacitors are similar, which may be due to the similar number of slow traps in capacitors. This situation makes qualitative comparison difficult, so we extract the values of V_{fb} of the *C*–*V* curves tested under different frequencies for a quantitative comparison. Given that the V_{fb} tested at 10 kHz is the smallest, we adopted it as the reference value in the quantitative calculation. $\Delta V_{fb-10\ K}$ was obtained from the following equation:

$$\Delta V_{fb-10\ K} = V_{fb-F} - V_{fb-10\ K}, \tag{1}$$

where V_{fb-F} is the V_{fb} tested at different frequencies, and $V_{fb-10\ K}$ is the V_{fb} tested at 10 kHz.

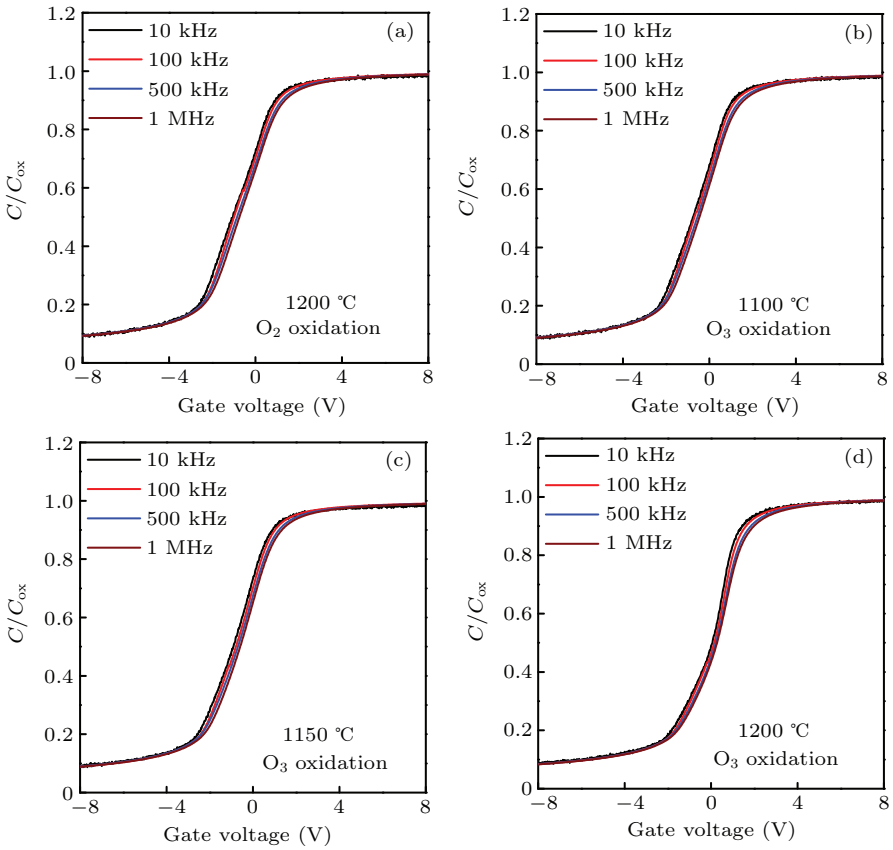


Fig. 2. The *C*–*V* curves of various SiC MOS capacitors under different test frequencies.

From Fig. 3, we observed that $\Delta V_{fb-10\ K}$ decreases with the increase in O_3 oxidation temperature, indicating that the higher the O_3 oxidation temperature is, the better the V_{fb} stability of the SiC MOS capacitors is during test frequency variation. Moreover, the sample formed by O_3 oxidation at 1200 °C has a smaller $\Delta V_{fb-10\ K}$ than the control sample. This finding signifies that the SiC MOS capacitor oxidized by O_3 at 1200 °C has better V_{fb} stability during test frequency variation than those oxidized by O_2 at the same temperature. We notice that the $\Delta V_{fb-10\ K}$ of the control sample is similar to that of the sample oxidized by O_3 at 1150 °C. The V_{fb} stability during test frequency variation of the sample obtained by dry oxidation at 1200 °C is only similar to that of the sample obtained by O_3 oxidation at 1150 °C.

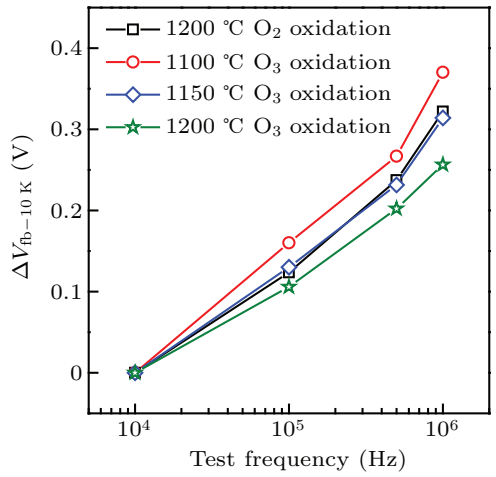


Fig. 3. Curves of $\Delta V_{fb-10\ K}$ *versus* test frequency of various SiC MOS capacitors.

3.3. Effect of test temperature on V_{fb}

Figure 4 shows our measured *C*–*V* curves of the SiC MOS capacitors in a temperature range of 80 K–300 K with a test frequency of 1 MHz. The *C*–*V* curves shift toward the accumulation region with the test temperature decreasing, which leads V_{fb} to shift. We extract $\Delta V_{fb-300\ K}$ from the following formula:

$$\Delta V_{fb-300\ K} = V_{fb-T} - V_{fb-300\ K}, \tag{2}$$

where V_{fb-T} is the V_{fb} at temperature T, and $V_{fb-300\ K}$ is the V_{fb} at 300 K. The results are shown in Fig. 5(a). We find that $\Delta V_{fb-300\ K}$ decreases with the increase in O_3 oxidation temperature. This result indicates that the increase of O_3 oxidation temperature can improve the V_{fb} stability of SiC MOS capacitors against test temperature variations. In addition, when the test temperature changes, the SiC MOS capacitors obtained by O_3 oxidation at 1200 °C show better V_{fb} stability than those formed by dry oxidation. Liu *et al.* reported that low temperature can reduce the difference between Fermi level (E_f) and the bottom of conduction band (E_c), so many interface traps near E_c are occupied by carriers with the decrease in temperature,[32] leading V_{fb} to shift. This result also means that a small D_{it} can provide good V_{fb} stability under test temperature variations. Subsequently, we calculated D_{it} in a range of 0.06 eV–0.18 eV under the values of E_c for various samples by using the Gray–Brown method.[33,34]

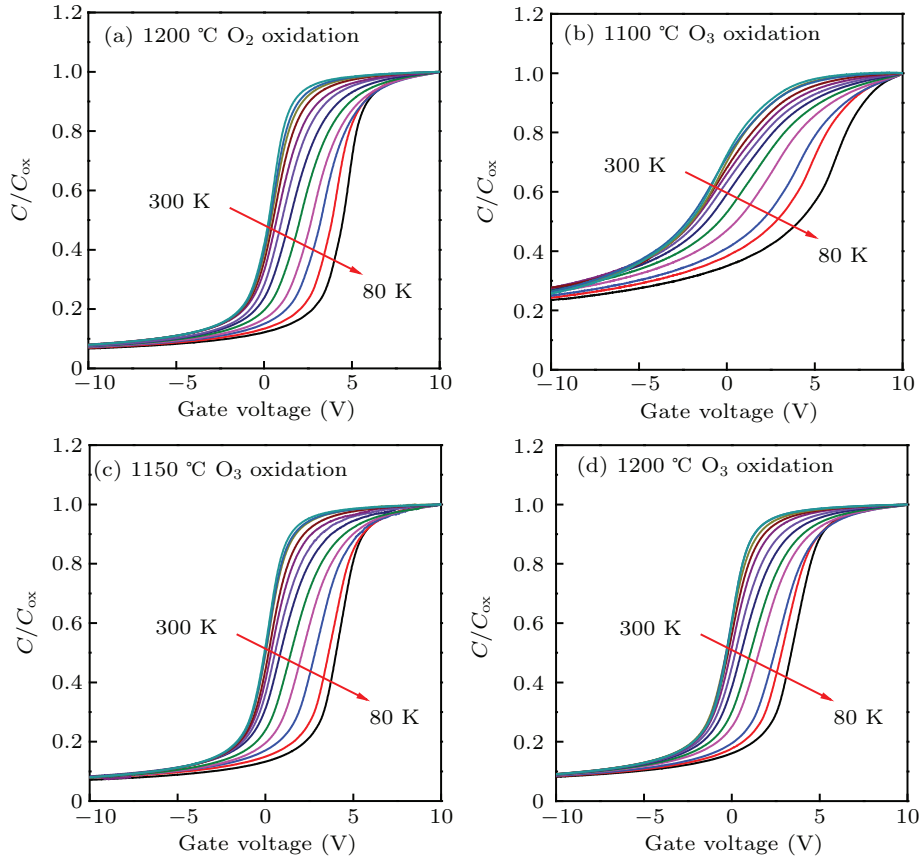


Fig. 4. The *C*–*V* curves of various SiC MOS capacitors under test temperatures in a range of 80 K–300 K.

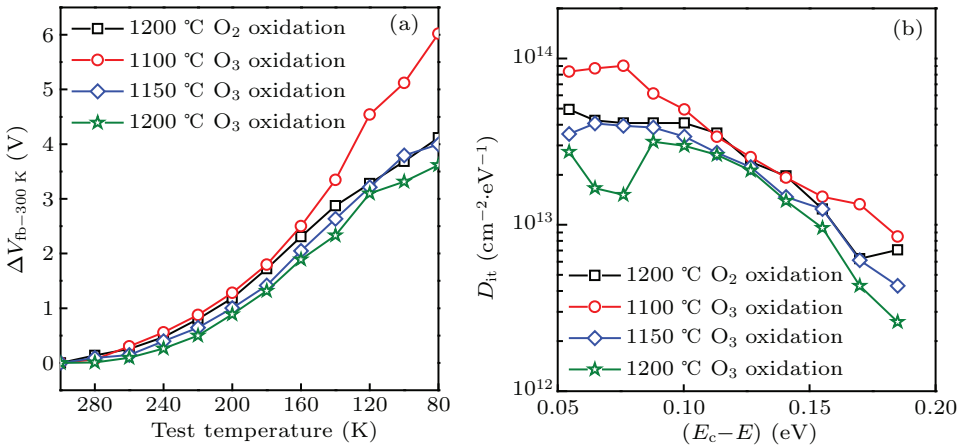


Fig. 5. Curves of (a) $\Delta V_{fb-300\ K}$ *versus* test temperature and (b) D_{it} *versus* (E_c–E) for SiC MOS capacitors prepared at four different temperatures.

As shown in Fig. 5(b), D_{it} in a range of 0.06 eV–0.18 eV decreases continuously with the increase in O_3 oxidation temperature. Compared with the D_{it} of the control sample, the D_{it} of the samples obtained by O_3 oxidation at the same temperature is reduced by nearly three quarters. The D_{it} of the control sample is only comparable to that of the samples formed by O_3 oxidation at 1150 °C. This result indicates that O_3 oxidation can effectively suppress the generation of interface traps at the SiC/SiO_2 interface, thereby improving the V_{fb} stability of SiC MOS capacitors.

3.4. The V_{fb} stability under BTS

The V_{fb} BTI of the SiC MOS capacitor is studied by testing the post-BTS *C–V* curves in a temperature range of 100 K–300 K. The *C–V* curves of post-BTS are shown in Figs. S1–S4 in supporting information. We extract the difference (ΔV_{fb}) in V_{fb} between post-positive-stress and post-negative-stress *C–V* curves, as shown in Fig. 6(a). We find that ΔV_{fb} increases with the decrease in test temperature for two reasons. First, many interface traps and NIOTs can be occupied by electrons due to the decrease in the difference between E_f and E_c, resulting from the decrease in test temperature.[9,34] Second, a low temperature can reduce the de-trapping rate of trapped carriers.[9,35] Therefore, the electrical signals of many traps can be tested by *C–V* curves. We observed that ΔV_{fb} decreases with the increase in O_3 oxidation temperature, indicating that V_{fb} BTI can be effectively improved by O_3 oxidation at high temperatures. In addition, we discovered that the ΔV_{fb} of the control sample is similar to that of the sample obtained by O_3 oxidation at 1100 °C. The V_{fb} stability of the control sample was only comparable to that of the sample obtained by O_3 oxidation at 1100 °C; it is obviously worse than that of the sample obtained by O_3 oxidation at 1200 °C. We realized that compared with dry oxidation, O_3 oxidation can be used to prepare SiC MOS capacitors with better V_{fb} stability. Sun *et al.* reported that a linear relationship exists between the difference (ΔV_{mg}) of V_{mg} between post-positive-stress and post-negative-stress *C–V* curves and the sum of mobile ions and oxide trap charges.[35] When they conduct *C–V* tests at low temperatures, the mobile ions hardly move, leading to a minimal influence on ΔV_{mg}.[9,36] Therefore, ΔV_{mg} only has a linear relationship with the oxide trap charge at low temperatures. We extract the values of ΔV_{mg} of the various SiC MOS capacitors for a quantitative analysis of NIOTs. As shown in Fig. 6(b), ΔV_{mg} decreases with the increase in the O_3 oxidation temperature.

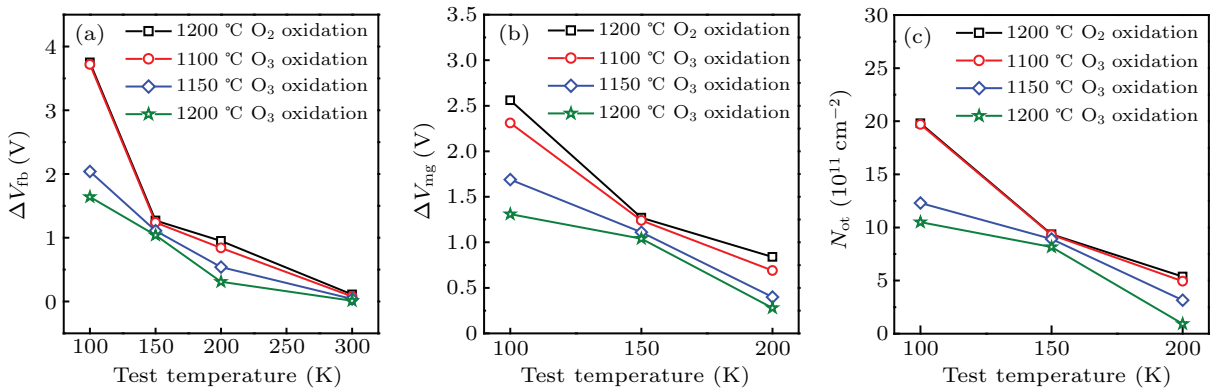


Fig. 6. Test temperature-dependent (a) ΔV_{fb}, (b) ΔV_{mg}, and (c) N_{ot} for SiC MOS capacitors prepared at four different temperatures.

Subsequently, we calculate the oxide trap amount (N_{ot}) from the following equation:[25,35]

$$N_{ot} = \frac{\Delta V_{mg} \times C_{ox}}{q}, \tag{3}$$

where C_{ox} is the oxide capacitance per unit area and q is the elementary charge. As shown in Fig. 6(c), we find that N_{ot} decreases with the increase in O_3 oxidation temperature, which means that SiC MOS capacitors with low N_{ot} can be prepared at a high O_3 oxidation temperature. In addition, we notice that the N_{ot} of the control sample is similar only to that of sample obtained by the O_3 oxidation at 1100 °C and larger than that of sample obtained by the O_3 oxidation, separately, at 1150 °C and 1200 °C. This result indicates that compared with dry oxidation, the O_3 oxidation can produce the SiC MOS capacitor with low N_{ot}, thereby improving the V_{fb} stability of SiC MOS capacitor.

According to the measurement results, the SiC MOS capacitor with similar V_{fb} stability can be produced by the O_3 oxidation at lower oxidation temperature than by the dry oxidation. A high O_3 oxidation temperature can effectively improve the V_{fb} stability of SiC MOS capacitor in a temperature range of 1100 °C–1200 °C. In addition, O_3 oxidation can produce SiC MOS capacitor with lower D_{it} and N_{ot} than by dry oxidation, thereby improving the V_{fb} stability of SiC MOS capacitor.

3.5. Element distribution near SiC/SiO_2 interface

Figure 7 shows the results of SIMS measurement, namely, the element distributions near the SiC/SiO_2 interfaces of different samples. The blue, black, and green dotted lines in Fig. 7 represent the boundary of the SiO_2 bulk, the SiC/SiO_2

interface, and the boundary of the SiC bulk, respectively.[34,37] The area between the SiO_2 bulk boundary and the SiC/SiO_2 interface represents the interface-transition region.[37] The peak of Si element content is observed in a part of the area between the SiC/SiO_2 interface and the boundary of the SiC bulk, which is called the Si-rich region and marked by red dotted lines in Fig. 7.[34] Previous reports have indicated that many defects exist in the interface-transition region and Si-rich region,[38] and they can influence the V_{fb} stability of SiC MOS capacitor by forming interface traps or NIOTs.[11,39–41] Therefore, studying the element distributions in these regions is essential to evaluate the possibility of defects.

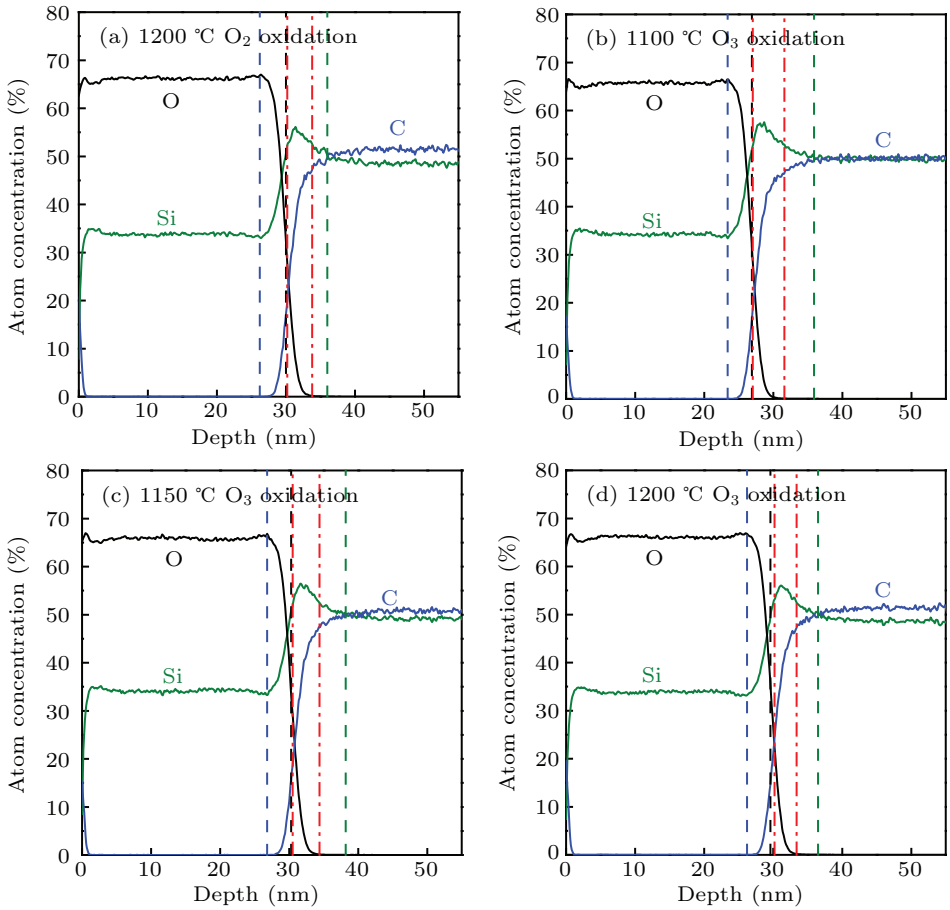


Fig. 7. Si, C, and O element depth profiles of various SiC/SiO_2 structures.

We extracted the thickness of the interface-transition and Si-rich region. Figure 8(a) shows the thickness of the interface-transition region in the different samples formed by O_3 and dry oxidation. The black dashed arrow in Fig. 8(a) indicates the thickness of the interface-transition region in the control sample. In addition, we calculate the relative Si and C element contents in the interface-transition region of the different samples, and the results are shown in Fig. 8(b). The blue and black dotted arrows represent the relative Si and C element contents in the interface-transition region of the control sample, respectively. As presented in Figs. 8(a) and 8(b), by comparing thickness and relative Si and C element contents of the interface-transition region of various samples, we examined the effect of O_3 oxidation on the interface-transition region. On the one hand, the thickness and relative Si and C element contents of the interface-transition region formed by O_3 oxidation are smaller than those of the interface-transition region formed by dry oxidation. On the other hand, the thickness and relative Si and C element contents of the interface-transition region decrease with the increase in O_3 oxidation temperature in a range of 1100 °C–1200 °C. The interface-transition region of the sample obtained by O_3 oxidation at 1200 °C is the thinnest, and its thickness is approximately 0.4 nm less than that of the samples formed by dry oxidation at the same oxidation temperature. Given that a thin interface-transition region and low Si and C element contents in the interface-transition region can reduce the existence possibility of Si- and C-related defects in the interface-transition region,[42] we infer that O_3 oxidation can suppress the formation of defects in the interface-transition region.

Figure 8(a) also shows the thickness of the Si-rich region in various samples. The blue dashed arrow in Fig. 8(a) indicates the thickness of the Si-rich region in the control sample. Figure 8(c) shows the Si and C element contents in the Si-rich region of different samples; the blue and black dotted arrows represent the Si and C element contents in the Si-rich region of the control sample, respectively. We notice that O_3 oxidation at high oxidation temperatures reduces the thickness of

the Si-rich region and the relative Si and C element contents in the Si-rich region. The thickness of the Si-rich region and the relative Si and C element contents in the Si-rich region of the samples formed by O_3 oxidation at 1100 °C and 1150 °C are greater than those of the control sample. Although O_3 oxidation at 1100 °C and 1150 °C can reduce the thickness and Si and C element contents of the interface-transition region, the thick Si-rich region and the large relative Si and C element contents of the Si-rich region limit the improvement of V_{fb} stability of the SiC MOS capacitors. In contrast to the above-mentioned capacitors, the SiC MOS capacitor formed by O_3 oxidation at 1200 °C has thinner interface-transition and Si-rich regions and lower relative Si and C element contents in the two regions. This result indicates that O_3 oxidation can limit the existence possibility of Si and C-related defects near the SiC/SiO_2 interface, and thus improves the V_{fb} stability of SiC MOS capacitors.

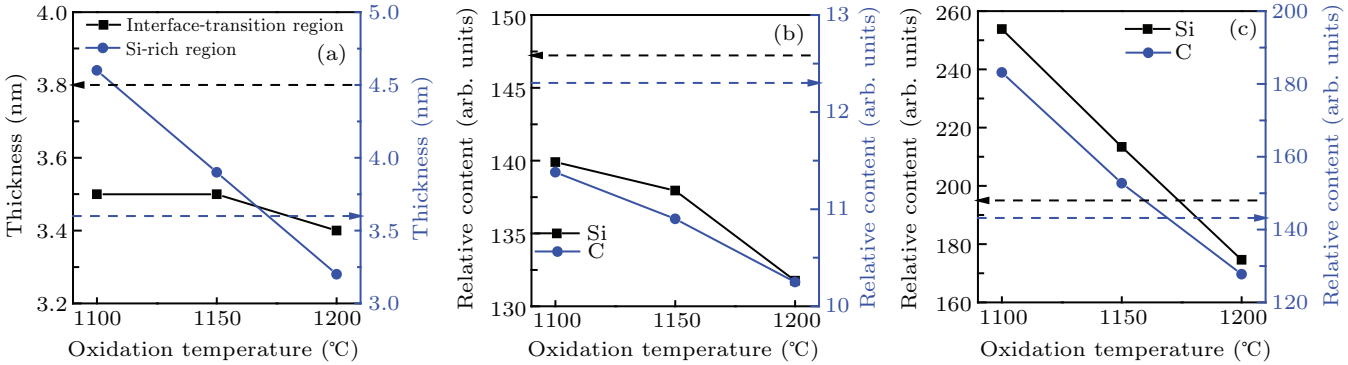


Fig. 8. (a) Plots of thickness *versus* oxidation temperature of interface-transition region and Si-rich region, with black dotted line and blue dotted line representing thickness of interface-transition region and Si-rich region of the control sample, respectively, (b) oxidation temperature-dependent relative Si and C element contents in interface-transition region, with black dotted line and blue dotted line denoting relative content of Si and C elements in interface-transition region and Si-rich region, respectively, and (c) oxidation temperature-dependent relative Si and C element contents in Si-rich region of SiC/SiO_2 structure obtained by O_3 oxidation, with black dotted line and blue dotted line referring to relative content of Si and C elements in interface-transition region and Si-rich region of the control sample, respectively.

3.6. Properties of SiC/SiO_2 interface

3.6.1. Interface morphology of SiC/SiO_2 interface

Figure 9 shows the SiC/SiO_2 interface morphologies of different samples from AFM measurements. The SiC/SiO_2 interface morphology obtained after O_3 oxidation is smoother than that after dry oxidation. The SiC/SiO_2 interface morphology becomes increasingly smooth with the increase in O_3 oxidation temperature. This trend is also observed from the roughness mean square (RMS) values of the SiC/SiO_2 interfaces of various samples. Previous reports have indicated that a smooth interface means few near-interface defects.[12,32]

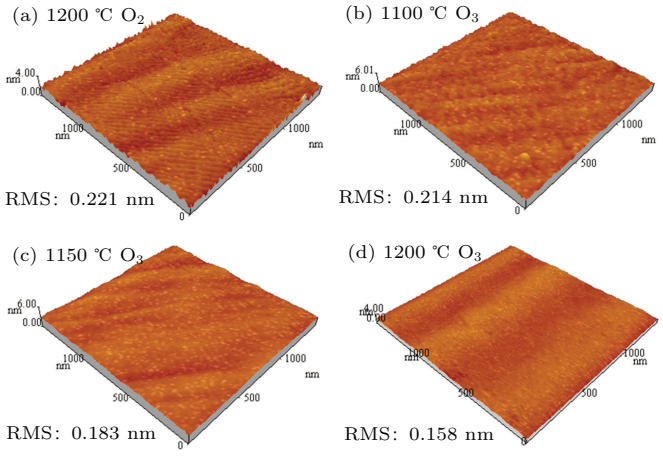


Fig. 9. Interface morphologies of SiC/SiO_2 structures obtained by (a) O_2 oxidation at 1200 °C and (b)–(d) O_3 oxidation at 1100 °C, 1150 °C, and 1200 °C, respectively.

We posit that the O_3 oxidation can improve the V_{fb} stability of SiC MOS device by making the SiC/SiO_2 interface smooth.

3.6.2. Element binding state of SiC/SiO_2 interface

Figure 10 shows the XPS Si 2p spectra of the SiC/SiO_2 interface obtained by dry the oxidation and O_3 oxidation. The binding energy values of the Si–C bond, SiO_xC_y, and Si–O bond in the XPS Si 2p spectra are 100.7 eV, 101.7 eV, and 103.1 eV, respectively.[39,43] The peak area of SiO_xC_y at the SiC/SiO_2 interface obtained by the dry oxidation at 1200 °C is similar to that obtained by the O_3 oxidation at 1100 °C. By contrast, the content of SiO_xC_y at the SiC/SiO_2 interface obtained by the O_3 oxidation at 1150 °C and 1200 °C are slightly reduced. This finding indicates that the O_3 oxidation has a limited effect on the generation of Si-related SiO_xC_y defects in the SiC MOS capacitor. Comparing with the control sample, the Si-related defects are reduced at 1150 °C and 1200 °C but still possess high content. Hence, we infer that the suppression of effect of O_3 oxidation on Si-related SiO_xC_y defects is limited.

The XPS C 1s spectra of the SiC/SiO_2 interface obtained by the dry oxidation and O_3 oxidation are shown in Fig. 11. In the XPS C 1s spectra, the binding energy values of the C–Si bond, C–SiO_x, and C–C bond are 282.5 eV, 283.7 eV, and 284.6 eV, respectively.[39,44] The C–SiO_x peak areas of the SiC/SiO_2 interface obtained by O_3 oxidation are obviously

smaller than those of the control sample, and the C–SiO_x peak areas decreases with the O_3 oxidation temperature increasing. This result indicates that O_3 oxidation can suppress the formation of C-related SiO_xC_y defects during oxidation. Notably, the C–C bond peak areas of the four samples are almost similar to each other, revealing that even if O_3 with strong oxidizability is used as the oxidation atmosphere, it can still result in the formation C–C defects from some C residues. Therefore, we infer that one of main ways through which O_3 oxidation can improve the V_{fb} stability of SiC MOS capacitor is to limit the generation of Si- and C-related SiO_xC_y defects.

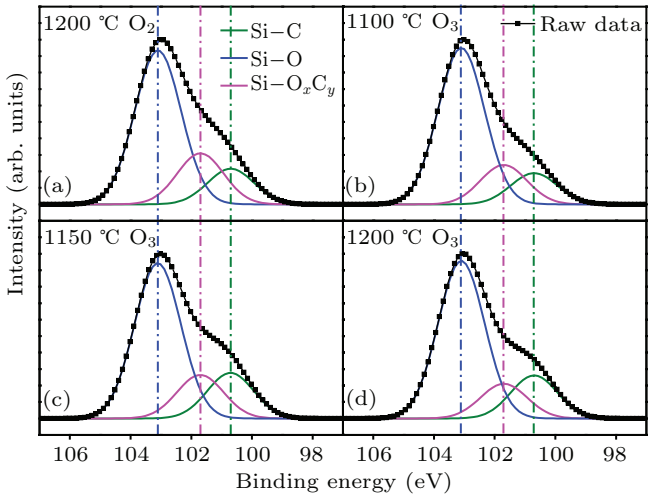


Fig. 10. Si 2p spectra of SiC/SiO_2 interface obtained by different oxidation methods.

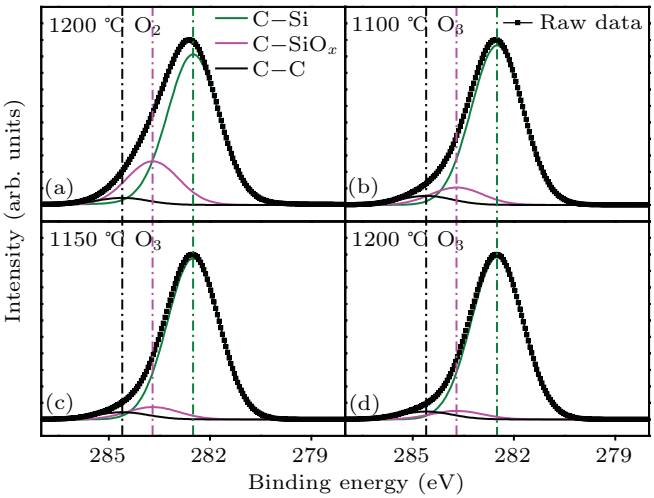


Fig. 11. C 1s spectra of SiC/SiO_2 interface obtained by different oxidation methods.

3.7. O_3 oxidation kinetics of (0001) Si-terminated face of 4H-SiC

We studied the kinetics of O_3 oxidation and dry oxidation to further ascertain the difference between O_3 oxidation and dry oxidation. We oxidized a 4H-SiC (0001) surface in O_2 or O_3 atmosphere in an oxidation temperature range of 1050 °C–1200 °C. Figures 12(a) and 12(b) show the relationships between dry oxidation time and O_3 oxidation time and thickness of SiO_2 film. The solid symbols and solid lines represent the experimental data and fitting curves from the modified Deal–Grove model, respectively. The modified Deal–Grove model is presented by Song *et al.* to describe the process of SiO_2 films growth on 4H-SiC by the dry oxidation.[27] In the modified Deal–Grove model of 4H-SiC, growth follows the following equation:[27,45,46]

$$X^2 + AX = B(t+\tau), \tag{4}$$

where X is the thickness of SiO_2 film, B is the parabolic rate constant, B/A is the linear rate constant, t is the oxidation time, and τ is related to the thickness of the primary oxide film. We extract B and B/A from Eq. (4).

Figures 12(c) and 12(d) show the relationship of the B and B/A of O_2 and O_3 oxidation with the oxidation temperature, respectively. We fit the experimental data of B and B/A by using the Arrhenius equation. We find that the activation energy of B and B/A for the dry oxidation are 3.12 eV and 1.32 eV, respectively, which are almost equivalent to the data obtained by Song *et al.*[27] By contrast, the activation energy of B and B/A of the O_3 oxidation are 3.79 eV and 2.31 eV, respectively, both of which are greater than those of the dry oxidation. Therefore, we would infer that SiO_2 film growth by O_3 oxidation is highly susceptible to the oxidation temperature. We notice that the B value of O_3 oxidation is greater than that of the dry oxidation in the oxidation temperature range of 1050 °C–1200 °C. Given that B has a positive relationship with the diffusion coefficient of O_2 and carbon monoxide (CO) gas,[27,47] we would infer that the rate of the oxidant internal diffusion and the CO external diffusion in the SiO_2 films during the O_3 oxidation of the 4H-SiC (0001) face are both higher than those during the dry oxidation. The O_3 can be decomposed into O_2 molecules and O atoms at high temperatures, and the O atoms have a high diffusion rate in SiO_2 film. In addition, we find little difference in B/A between the dry oxidation and the O_3 oxidation at temperatures in a range of 1050 °C–1200 °C in Fig. 12(d), which may be due to the fact that the main factor that influences the initial interfacial reaction rate is the breakage of the Si–C bond.[47] Therefore, we would infer that the O_3 oxidation can suppress the formation of near-interface defects by releasing O atoms,[26,48] which can increase the diffusion rate of the oxidant in the SiO_2 film and the concentration of the oxidant at the SiC/SiO_2 interface, thereby promoting a complete oxidation reaction and reducing defects near the SiC/SiO_2 interface.

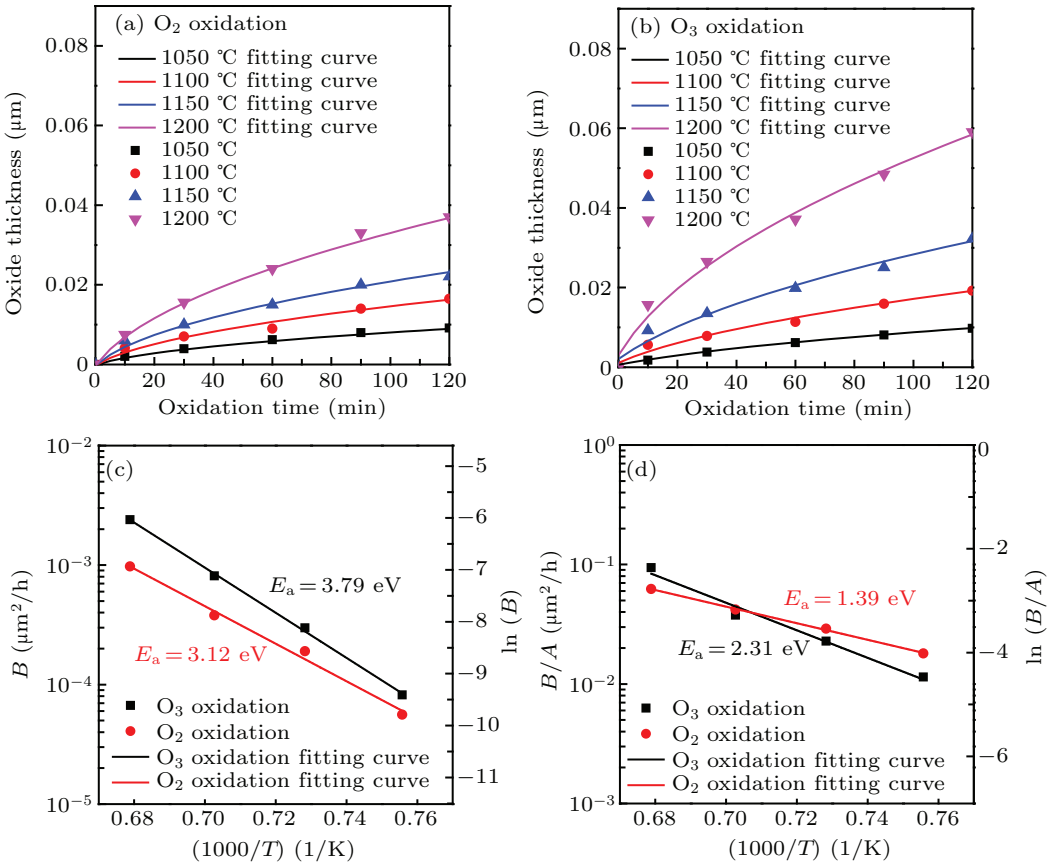


Fig. 12. Plots of oxide thickness *versus* (a) O_2 oxidation time and (b) O_3 oxidation time for (0001) Si-terminated face of 4H-SiC prepared at different temperatures, with solid lines indicating fits by Eq. (4). (c) Arrhenius plots for Deal–Grove parabolic rate constant B, with activation energy found to be 3.12 eV and 3.79 eV for O_2 and O_3 oxidations of Si faces, respectively. (d) Arrhenius plots for Deal–Grove parabolic rate constant B/A, with activation energy found to be 2.31 eV and 1.39 eV for O_2 and O_3 oxidations of Si faces, respectively.

3.8. Mechanism of V_{fb} stability improvement by O_3 oxidation

We analyzed the underlying mechanism through which O_3 oxidation improves the V_{fb} stability of the SiC MOS capacitor, by combining the measurement results and the modified Deal–Grove model. It is noticed that O_3 can be decomposed into O atoms that have high diffusion rate in SiO_2 films and high oxidizability,[20,26] which can promote the complete oxidation of SiC at the SiC/SiO_2 interface. The measurement results indicate that O_3 oxidation can reduce the thickness and relative Si and C element contents of the interface-transition and Si-rich regions, thereby reducing the existence possibility of Si- and C-related defects near the SiC/SiO_2 interface. In addition, O_3 oxidation also effectively suppresses the formation of SiO_xC_y at the SiC/SiO_2 interface, and smooths the SiC/SiO_2 interface. These behaviors can restrain the formation of interface traps and NIOTs, thereby improving the V_{fb} stability of SiC MOS capacitor. With the increase in O_3 oxidation temperature, these optimization behaviors can become increasingly obvious. Therefore, in this study, the SiC MOS capacitor obtained by O_3 oxidation at 1200 °C possesses lower D_{it} and N_{ot}, thereby making the V_{fb} stability of these SiC MOS capacitors better than those of the other samples.

4. Conclusions

In this work, we studied the effect of O_3 oxidation on the V_{fb} stability of SiC MOS capacitor and analyzed the difference between O_3 oxidation and dry oxidation. We found that the SiC MOS capacitor obtained by O_3 oxidation has slighter frequency dispersion, better temperature stability, and more acceptable BTI characteristics than the samples obtained by dry oxidation at the same oxidation temperature. The O_3 oxidation can produce the SiC MOS capacitor with similar V_{fb} stability but at a low temperature compared with the traditional dry oxidation. The measurement results of SIMS, AFM, and XPS showed that the O_3 oxidation reduces the thickness and relative Si and C element contents of the interface-transition region and Si-rich region, and thus reducing the possibility of creating the Si- and C-related defects near the SiC/SiO_2 interface. Moreover, the O_3 oxidation suppresses the formation of SiO_xC_y defects and reduces the roughness of the SiC/SiO_2 interface. Consequently, the O_3 oxidation can reduce the D_{it} and N_{ot} of the SiC MOS capacitor, thereby improving the V_{fb} stability of the capacitor. The underlying mechanism is elucidated by examining the O_3 oxidation kinetics, which proves that O_3 can more easily diffuse in SiO_2 film than O_2 due to the release of O atoms, and thus promoting a complete interface reaction. In addition, we found that the increasing of

the O_3 oxidation temperature can improve the quality of the near-interface region and optimize the V_{fb} stability of the SiC MOS capacitor. Notably, the V_{fb} stability of SiC MOS capacitor formed by O_3 oxidation can be further improved by combining this approach with other POA methods.

Acknowledgement

Project supported by the National Natural Science Foundation of China (Grant No. 61874017).

References

[1] She X, Huang A Q, Lucia O and Ozpineci B 2017 *IEEE Transactions on Industrial Electronics* **64** 8193
[2] Liu G, Tuttle B R and Dhar S 2015 *Appl. Phys. Rev.* **2** 021307
[3] Yang C, Wei S and Wang D 2021 *J. Phys. D: Appl. Phys.* **54** 123002
[4] Matocha K 2008 *Solid-State Electron.* **52** 1631
[5] Chung G Y, Tin C C, Williams J R, McDonald K, Ventra M D, Pantelides S T, Feldman L C and Weller R A 2000 *Appl. Phys. Lett.* **76** 1713
[6] Jamet P and Dimitrijev S 2001 *Appl. Phys. Lett.* **79** 323
[7] Aichinger T, Rescher G and Pobegen G 2018 *Microelectronics Reliability* **80** 68
[8] Zhang F, Yang C, Su Y and Wang D 2020 *Appl. Surf. Sci.* **514** 145889
[9] Yang C, Gu Z, Yin Z, Qin F and Wang D 2019 *J. Phys. D: Appl. Phys.* **52** 405103
[10] Zhang Y J, Yin Z P, Su Y and Wang D J 2018 *Chin. Phys. B* **27** 047103
[11] Li W, Li L, Wang F, Zheng L, Xia J, Qin F, Wang X, Li Y, Liu R, Wang D, Pan Y and Yang F 2017 *Chin. Phys. B* **26** 037104
[12] Jia Y, Lv H, Song Q, Tang X, Xiao L, Wang L, Tang G, Zhang Y and Zhang Y 2017 *Appl. Surf. Sci.* **397** 175
[13] Liu P, Hao J L, Wang S K, You N N, Hu Q Y, Zhang Q, Bai Y and Liu X Y 2021 *Chin. Phys. B* **30** 077303
[14] Knaup J M, Deák P, Frauenheim T, Gali A, Hajnal Z and Choyke W J 2005 *Phys. Rev. B* **71** 115323
[15] You N, Liu X, Bai Y, Liu P, Zhang Q, Zhang Y and Wang S 2021 *Appl. Surf. Sci.* **562** 150165
[16] Li W, Zhao J, Zhu Q and Wang D 2013 *Phys. Rev. B* **87** 085320
[17] Indari E D, Yamashita Y, Hasunuma R, Oji H and Yamabe K 2019 *AIP Adv.* **9** 105018
[18] Liu X, Hao J, You N, Bai Y and Wang S 2019 *AIP Adv.* **9** 125150
[19] Liu X Y, Hao J L, You N N, Bai Y, Tang Y D, Yang C Y and Wang S K 2020 *Chin. Phys. B* **29** 037301
[20] Kosugi R, Fukuda K and Arai K 2003 *Appl. Phys. Lett.* **83** 884
[21] Ebihara Y, Chokawa K, Kato S, Kamiya K and Shiraishi K 2012 *Appl. Phys. Lett.* **100** 212110
[22] Shirakawa H, Kamiya K, Araidai M, Watanabe H and Shiraishi K 2016 *Appl. Phys. Express* **9** 064301
[23] Yoshioka H, Nakamura T and Kimoto T 2012 *J. Appl. Phys.* **112** 024520
[24] Kim D K, Jeong K S, Kang Y S, Kang H K, Cho S W, Kim S O, Suh D, Kim S and Cho M H 2016 *Sci. Rep.* **6** 34945
[25] Yin Z, Wei S, Bai J, Xie W, Qin F and Wang D 2021 *Ceram. Int.* **48** 10874
[26] Fink C K, Nakamura K, Ichimura S and Jenkins S J 2009 *J. Phys.: Condens. Matter* **21** 183001
[27] Song Y, Dhar S, Feldman L C, Chung G and Williams J R 2004 *J. Appl. Phys.* **95** 4953
[28] Kodigala S R, Chattopadhyay S, Overton C and Ardoin I 2015 *Solid-State Electron.* **114** 104
[29] Ettisserry D P, Goldsman N and Lelis A J 2017 *IEEE Trans. Electron Dev.* **64** 1007
[30] Peng Z, Wang Y, Shen H, Li C, Wu J, Bai Y, Liu K and Liu X 2016 *Microelectronics Reliability* **58** 192
[31] Peng Z Y, Wang S K, Bai Y, Tang Y D, Chen X M, Li C Z, Liu K A and Liu X Y 2018 *J. Appl. Phys.* **123** 135302
[32] Liu B, Qin F and Wang D 2016 *Appl. Surf. Sci.* **364** 769
[33] Gray P V and Brown D M 1966 *Appl. Phys. Lett.* **8** 31
[34] Zhu Q, Qin F, Li W and Wang D 2014 *Physica B* **432** 89
[35] Sun Y, Chao Y, Yin Z, Qin F and Wang D 2019 *J. Appl. Phys.* **125** 185703
[36] Chanthaphan A, Hosoi T, Nakano Y, Nakamura T, Shimura T and Watanabe H 2013 *Appl. Phys. Lett.* **102** 093510
[37] Zhu Q, Qin F, Li W and Wang D 2013 *Appl. Phys. Lett.* **103** 062105
[38] Shen X and Pantelides S T 2011 *Appl. Phys. Lett.* **98** 053507
[39] Zhu Q, Huang L, Li W, Li S and Wang D 2011 *Appl. Phys. Lett.* **99** 082102
[40] Li W, Zhao J and Wang D 2015 *AIP Adv.* **5** 017122
[41] Li W, Zhao J and Wang D 2015 *Solid State Commun.* **205** 28
[42] Yin Z, Yang C, Zhang F, Su Y, Qin F and Wang D 2020 *Appl. Surf. Sci.* **531** 147312
[43] Kobayashi H, Sakurai T, Takahashi M and Nishioka Y 2003 *Phys. Rev. B* **67** 115305
[44] Yang C, Zhang F, Yin Z, Su Y, Qin F and Wang D 2019 *Appl. Surf. Sci.* **488** 293
[45] Deal B E and Grove A S 1965 *J. Appl. Phys.* **36** 3770
[46] Heihachiro Kikuchi R and Kita K 2014 *Appl. Phys. Lett.* **104** 052106
[47] Goto D, Hijikata Y, Yagi S and Yaguchi H 2015 *J. Appl. Phys.* **117** 095306
[48] Kosugi R, Ichimura S, Kurokawa A, Koike K, Fukuda K, Suzuki S, Okushi H, Yoshida S and Arai K 2000 *Appl. Surf. Sci.* **159–160** 550